Electrical Power and Energy Systems 158 (2024) 109922

Contents lists available at ScienceDirect

International Journal of Electrical Power and Energy Systems

journal homepage: www.elsevier.com/locate/ijepes

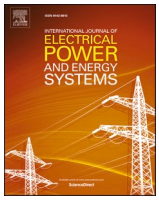

Improving the time delay in the design of the damping controller with the aim of improving the stability of the power system in the presence of high penetration of renewable energy sources

Shuguang Li [a], Mohana Alanazi [b,*], Rasheed Abdulkader [c], Mohamed Salem [d,e], Maher G.M. Abdolrasol [f], Faisal A Mohamed [e], Thamer A.H. Alghamdi [g,h,*]

[a] School of Computer Science and Technology, Shandong Technology and Business University, Yantai 264005, China
[b] Department of Electrical Engineering, College of Engineering, Jouf University, Sakaka 72388, Saudi Arabia
[c] Department of Electrical Engineering, Imam Mohammad Ibn Saud Islamic University (IMSIU), Riyadh, Saudi Arabia
[d] School of Electrical and Electronic Engineering, Universiti Sains Malaysia (USM), Nibong, Tebal 14300, Penang, Malaysia
[e] Libyan Authority for Scientific Research, Tripoli, Libya
[f] Institute of Sustainable Energy, Universiti Tenaga Nasional, Kajang 43000, Malaysia
[g] Wolfson Centre for Magnetics, School of Engineering, Cardiff University, Cardiff CF24 3AA, UK
[h] Electrical Engineering Department, Faculty of Engineering, Al-Baha University, Al-Baha 65779, Saudi Arabia

ARTICLE INFO

Keywords:
Linear matrix inequality
Free weight matrices
Wide area damping controller
Battery energy storage system

ABSTRACT

Due to the high penetration of renewable energy sources (RES) such as wind units in power systems, the need to check the stability of transmission networks has been given more attention than before. Therefore, in this paper, due to the importance of the topic, the wide area damping controller (WADC) has been used for the battery energy storage system (BESS) connected to the photovoltaic unit and the permanent magnet synchronous generator (PMSG) in the dc link. The WADC design is based on free weight matrices (FWM), which can solve a set of constraints based on the linear matrix inequality (LMI) based on the delay-dependent feedback control theory. The working method is that the constraints related to LMI are considered in such a way that it has the ability to tolerate the maximum amount of time delay. FWM has been used to communicate between LMI constraints and the maximum value of the time delay margin. FWM matrices are also based on an iterative algorithm based on linearization of the conical complement, which tries to search for the most optimal value for the control parameters. To implement the simulation results in MATLAB software, an improved power system of 16 machines has been used, the results of which are clearly analyzed and show the superiority of the proposed method compared to other mentioned methods.

1. Introduction

Due to the high penetration of RES in power systems, the need to reduce the fluctuations caused by RES is more important than before, so that it is necessary to control the fluctuating modes of the power network through the design of supplementary controllers [1,2]. Due to the importance of power system oscillation damping, the modes that are in the frequency range of 0.2 to 0.9 Hz are called local modes and the modes that are in the frequency range of 0.9 to 2 Hz are called inter-regional modes [2,3]. In this regard, the design of supplementary controllers are also divided into two local categories, including power system stabilizers (PSS) installed on synchronous generators (SG) and global as power oscillation damping (POD) [4,5]. Among the types of RES, the use of PV and wind power plants has been more common than other RES due to having modern technologies and combined operation with each other [6]. But in addition to using more of these resources, other problems due to the random pattern of wind blowing and solar radiation intensify the power system's oscillating modes. In this regard, the WADC design greatly contributes to the stability of the power system due to the control of inter-area modes [7,8]. But considering that WADC damping signals are sent from different and distant areas of the power system, there is a possibility of time delays in sending these signals to the control centers. Therefore, the main idea of recent research in various references is related to the compensation of time delays of signals sent

* Corresponding authors.
E-mail addresses: msanazi@ju.edu.sa (M. Alanazi), Alghamdit1@cardiff.ac.uk (T.A.H. Alghamdi).

https://doi.org/10.1016/j.ijepes.2024.109922
Received 24 November 2023; Received in revised form 29 January 2024; Accepted 4 March 2024
Available online 16 March 2024

through phasor measurement units (PMU) to PODs or PSSs. Therefore, compensating the time delay in sending damping signals to POD or PSS is very important to improve the stability of the power system.

In [9], multi-model adaptive control is used to design POD in a PV, in which a clustering algorithm is introduced to identify inter-area modes under different operating conditions. In [10], POD design for a BESS based on small signal stability and torque-electric method is reported. So that their main goal is to reduce inter- area fluctuations based on optimization of POD parameters based on Markov model and reinforcement learning. In [11], a sensor sensitive to inter- area frequencies is used to reduce the range of fluctuations in the path of input feedback signals. Through this sensor, critical inter- area frequencies can be identified and then to compensate for weak modes, damping signals are sent to the POD input. In [12], real-time damping ratio and reference value were compared in a single-input–single-output nonlinear model using the continuous state estimation method, and based on the result of this comparison, the parameters of the damping controller were designed for an interface converter. In [13], the step-down modulation method is used for active power modulation. In this method, after detecting a transient event, the PV panel voltage is controlled to prevent the transient power deviation through maximum power point tracking (MPPT) and continues until the fluctuation is not reduced. The hybrid particle swarm optimization method is a simple yet practical method that has been used to optimize WADC controller parameters in the presence of time delays in various researches [14]. Among other optimization methods, we can refer to the reinforcement learning method based on policy gradient using neural networks [15]. However, in this method, because the system model is not available, a very extensive discretization operation is needed to identify it. Analysis of dynamic modes based on an online model is a method introduced in the measurement of WADC signals in [16]. The basis of this method is based on singular value decomposition (SVD). This depends on the accurate low-order model in the dynamics of the power system. Using SVD to reduce the order of power system and design with discrete linear quadratic regulator (LQR) for WADC controller is a method introduced without considering time delay in [16]. Network Predictive Control (NPC) is another online model identification method that is introduced in the WADC design for the rotor side converter (RSC) of a wind farm [17]. One of the important advantages of NPC is considering the physical constraints of the system in the online optimization process. However, in order for the prediction of system outputs to be valid, it is necessary to be very careful in identifying the online model of the plant. In WADC design, it is very important to try to increase the delay margin to compensate for the time delay. Based on this, in [18], the delay margin has been designed for second-order oscillatory modes with respect to fixed delays, square wave and gamma distribution. In this design method, a probability distribution function is used in order to be able to consider the special values of the oscillatory modes in the presence of random delays. However, no method is considered for the distribution of the probability function.

The use of Lyapunov functions is another problem solving method in order to prove stability, which can be effectively useful in WADC design. The stability guarantee of the Lyapunov function, which can be proved by its negative derivative, can be rewritten through the LMI criterion. The design by LMI for WADC can stabilize the inter-area fluctuations in a range of delay changes, in other words, the design method in LMI is such that it avoids the changes of unbalanced strategies in the control system [19]. But the structure of Lyapunov functions is one of the basic factors for high conservatism in the LMI criterion. Therefore, the design of a suitable Lyapunov function should include variables that, in addition to maintaining the degree of conservatism of LMI, also have the necessary stability. In [20], Pad approximation is used as delay modeling in LMI for WADC design where only fixed delays are controlled. In [21,22], the process of solving the LMI problem is based on time-varying delays, which are entered into the controller by feedback output signals. But in solving their problem, there are no additional variables and cross terms in the structure of the Lyapunov function, so that the delay with a long range is easily replaced by its boundaries, and as a result, it is not possible to accurately trace the existence of the delay with time.

In [23], the design of the robust damper controller for the power system is transformed into a general H_∞ problem and solved by the LMI method, but the selection of the optimal weight parameters for the H_∞ controller is difficult. Based on the above studies, in this paper, an improved optimal control method based on the FWM approach is used to design the WADC, which has the ability to effectively compensate for time delays. Therefore, the main purpose of the damping controller in this paper is to be able to damp the inter-area modes through the WADC in the BESS converter. Based on this, first the remote signals are determined by the visibility and controllability index and then it enters the FWM design process as a $u(t-\tau) = Kx(t-\tau)$ signal. Finally, based on the response obtained from the design method, damping signals can be applied to the BESS control loop along with time delay compensation.

Briefly, the innovations of this paper are presented under the following comments:

- New FWM design to compensate for the uncertainty caused by continuous and disruptive time delays.
- Adapting the FWM method to the LMI in the form of an optimization problem.
- Combined modeling of energy storage system with RES in large-scale power system.

2. Wide area damping controller design

In the design of damping controllers as WADC, selection of input control signals is done based on small signal analysis or other methods. Therefore, it should be noted that the application of wide area measurement systems (WAMS) to transmit global signals inevitably causes a time delay, and therefore the operation of the power system with WAMS is a kind of time delayed system. For this purpose, in this work, Pade's first-order approximation along with the use of high-pass and low-pass filters have been used to model the time delay. In this work, in addition to compensating the time delay, the K gain related to the state feedback control matrix has been optimally extracted using FWM. On the other hand, the gain matrix K is for the state variables and the state variables cannot be fully observed in practical power systems. Therefore, in this work, the state observer $O(s)$ has been introduced to observe the state variables based on pole placement, so that a more accurate response can be made from the controller design.

2.1. A. Free weight matrix method

Delay-dependent and delay-independent criteria are two types of criteria for controllers related to delayed systems that are discussed in control theory discussions. Considering that the delay-dependent measure uses delay size information, but the delay-independent stability measure does not need this information; Therefore, the delay-dependent criterion usually has a lower degree of conservatism than the delay-independent criterion, and it becomes more prominent when the time delays are small. The Lyapunov method is a main method for deriving the delay-dependent criterion, in which the discretized Lyapunov is one of the most efficient methods, but combining this method with the control system is very difficult and complicated. Another method is to transform the fixed model, one of the most effective and practical of which is the combined method of Park's and Moon's inequalities, whose preliminary model is presented in reference [24,25]. However, extensive research in this field continues. Therefore, the FWM method is proposed as a new method to solve the stability problem in many delayed systems. For the controller design based on the FWM method, the conservatism degree of the controller is reduced compared to the fixed model transformation methods. In the invariant model transformation, when the derivative of the Lyapunov function is calculated, some inequalities such as Park's and Moon's are used to estimate the

upper bound of the cross terms. In contrast, the FWM method does not require bounding techniques for some cross terms. To illustrate this, a common stability problem for a delayed system is considered as follows (1):

$$\dot{x}(t) = Ax(t) + Bx(t-\tau) + Cu(t) \tag{1}$$

In eq. (1), constants A, B, and C are constant real matrices with appropriate dimensions. In (1), τ represents the time delay and u(t) represents the input control signal. In this paper, to express the problem, first, the Lyapunov function is described according to (2):

$$V(t,x_t) = x^T(t)Px(t) + \int_{t-\tau}^{t} x^T(s)Qx(s)ds + \int_{-\tau}^{0}\int_{t+\theta}^{t} \dot{x}^T(s)Z\dot{x}(s)dsd\theta \tag{2}$$

In eq. (2), the first and second terms of the Lyapunov function are considered as potential to kinetic energy quantities in mechanical systems, and the third term is used for derivation. $P = P^T, Q = Q^T, Z = Z^T$ expressions should be determined and then the derivative of the Lyapunov function should be calculated as (3):

$$\begin{aligned}\dot{V}(x_t) =& \dot{x}^T(t)Px(t) + x^T(t)P\dot{x}(t) + x^T(t)Qx(t) - x^T(t-\tau)Qx(t-\tau) \\ &+ \tau\dot{x}^T(t)Z\dot{x}(t) - \int_{t-\tau}^{t} \dot{x}^T(s)Zx(s)ds\end{aligned} \tag{3}$$

In order to provide the LMI-based stability criterion, using the conventional stationary model transformation and Lyapunov theory, the right-hand side of eq. (4) is usually added to the $V(t,x_t)$ derivative in (3). Based on this, we will have (4):

$$0 = 2x^T(t)PB\left[x(t) - x(t-\tau) - \int_{t-\tau}^{t} \dot{x}(s)ds\right] \tag{4}$$

Where B is the matrix of coefficients and P is the Lyapunov matrix.

One of the limitations of solving the problem in classical methods such as transforming the time-invariant model to establish the $\dot{V}(x_t) < 0$ condition is the adjustment of matrices B and P, which cannot be determined freely. Therefore, when using the derivative of the Lyapunov function, in order to reduce the degree of conservatism, instead of directly using B and P, two new FWMs M and N can be used in the New Leibniz formula. According to this, calculating the derivative of eq. (3) is equivalent to adding the right side of eq. (5) to $\dot{V}(x_t) < 0$. Then we can provide some LMI inequalities to satisfy the condition. Based on this, we will have:

$$0 = [x^T(t)M + \dot{x}^T(t)N]\left[x(t) - x(t-\tau) - \int_{t-\tau}^{t} \dot{x}(s)ds\right] \tag{5}$$

So, as seen in the FWM method, there is no need to choose B and P, and it is enough to optimize M and N by solving the LMIs, so the FWM method reduces the degree of conservatism of the controller for the time delay system.

2.2. B. Mathematical modeling for WADC design based on FWM method

In this paper, the power system model (including generators, loads, PV and wind units and various controllers) is described using differential algebraic equations. In this way, the open loop system is modeled first, for this purpose, the output of the complementary BESS controller is used as input and the wide area control signals are used as the output of the open loop power system. Furthermore, when the time delay is used as the transmission delay for the WADC controller input, the linearized system model is expressed as (6):

$$\begin{cases}\dot{x}(t) = Ax(t) + Bu(t-\tau) \\ y(t) = Cx(t)\end{cases} \tag{6}$$

Where A, B, and C are state, input, and output matrices, respectively. In the following, the state feedback controller is expressed as (7):

$$u(t-\tau) = Kx(t-\tau) \tag{7}$$

Based on the open loop system expressed in (5) and the controller model in (6), the closed loop system model can be described as (8):

$$\begin{cases}\dot{x}(t) = Ax(t) + BKu(t-\tau) \\ y(t) = Cx(t)\end{cases} \tag{8}$$

The purpose of this section is to provide a delay-dependent stability criterion in the new model to optimally provide the controller gain in the presence of time delay, so that the closed-loop system of eq. (8) remains stable. Therefore, with the definition of Lemma 1, we will have:

Lemma 1 (Schur's complement [26]): for a symmetric matrix ($r = r^T = \begin{bmatrix} r_{11} & r_{12} \\ r_{21} & r_{22}\end{bmatrix}(r_{11} \in \Re^{r\times r})$), the following three conditions hold:

1. $r < 0$
2. $r_{11} < 0, r_{22} - r_{12}^T r_{11}^{-1} r_{12} < 0$
3. $r_{22} < 0, r_{11} - r_{12}^T r_{22}^{-1} r_{12}^T < 0$

Theorem 1: For a given scalar h, there will exist a state feedback controller *according to (7) for which the closed-loop system (8) remains stable, provided there are* $Y = \begin{bmatrix} Y_{11} & Y_{12} \\ Y_{21} & Y_{22}\end{bmatrix} \geqslant 0, L = L^T > 0, Q_1 = Q_1^T > 0,$ $R = R^T > 0$ *and matrices* M_1, M_2, *and* V *such that satisfy matrix inequalities (9) and (10):*

$$\Phi = \begin{bmatrix} AL + LA^T + M_1 + M_1^T + Q_1 + hY_{11} & BV - M_1 & hLA^T \\ * & -M_2 - M_2^T & hV^TB^T \\ * & * & -hR \end{bmatrix} < 0 \tag{9}$$

$$\Psi = \begin{bmatrix} Y_{11} & Y_{12} & M_1 \\ * & * & -M_2 \\ * & * & LR^{-1}L \end{bmatrix} > 0 \tag{10}$$

Where the sign * indicates the symmetry of the matrix and $K = VL^{-1}$ the gain of the feedback controller.

Proof: According to the Newton-Leibniz formula, we have (11):

$$x(t) - x(t-\tau) - \int_{t-\tau}^{t} \dot{x}(s)ds = 0 \tag{11}$$

According to (10), for every matrix with appropriate dimensions N_1 and N2, eq. (12) is satisfied:

$$0 = 2(x^T(t)N_1 + x^T(t-\tau)N_2) \times \left[x(t) - x(t-\tau) - \int_{t-\tau}^{t} \dot{x}(s)ds\right] \tag{12}$$

In the definition of any semi-positive definite matrix such as $Y = \begin{bmatrix} X_{11} & X_{12} \\ X_{12}^T & X_{22}\end{bmatrix} \geqslant 0$, eq. (13) can be satisfied:

$$h\xi^T(t)X\xi(t) - \int_{t-\tau}^{t} \xi^T(t)X\xi(t)ds > 0 \tag{13}$$

$$\xi(t) = [x^T(t), x^T(t-\tau)]^T$$

Now, by constructing the candidate Lyapunov function, we will have eq. (14):

$$V(x_t) = x^T(t)Px(t) + \int_{t-\tau}^{t} x^T(s)Qx(s)ds + \int_{-h}^{0}\int_{t+\theta}^{t} \dot{x}^T(s)Z\dot{x}(s)dsd\theta \tag{14}$$

Where $P = P^T > 0, Q = Q^T > 0, Z = Z^T > 0$ should be determined.

Then, by calculating the derivative of $V(x_t)$ in eq. (14) for system (8), we will have (15):

$$\begin{aligned}\dot{V}(x_t) &= \dot{x}^T(t)Px(t) + x^T(t)P\dot{x}(t) + x^T(t)Qx(t) - x^T(t-\tau)Qx(t-\tau) + h\dot{x}^T(t)Z\dot{x}(t) - \int_{t-h}^{t}\dot{x}^T(s)Z\dot{x}(s)ds \\ &= x^T(t)[PA + A^TP]x(t) + 2x^T(t)PBKx(t-\tau) + x^TQx(t) - x^T(t-\tau)Qx(t-\tau) \\ &+h[Ax(t) + BKx(t-\tau)]^TZ[Ax(t) + BKx(t-\tau)] - \int_{t-h}^{t}\dot{x}^T(s)Z\dot{x}(s)ds\end{aligned} \tag{15}$$

Next, by adding the right-hand side of eqs. (12) and (13) to $\dot{V}(x_t)$, eq. (16) is derived:

$$\begin{aligned}&\dot{V}(x_t) = x^T(t)[PA + A^TP]x(t) + 2x^T(t)PBKx(t-\tau) + x^TQx(t) - x^T(t-\tau)Qx(t-\tau) + h[Ax(t) + BKx(t-\tau)]^T \\ &Z[Ax(t) + BKx(t-\tau)] + h\xi^T(t)X\xi(t) + 2(x^T(t)N_1 + x^T(t-\tau)N_2)[x(t) - x(t-\tau)] - \int_{t-\tau}^{t}\dot{x}^T(s)Z\dot{x}(s)ds \\ &- \int_{t-\tau}^{t}\xi^T(t)X\xi(t)ds - 2[x^T(t)N_1 + x^T(t-\tau)N_2]\int_{t-\tau}^{t}\dot{x}(s)ds = x^T(t)[PA + A^TP + hA^TZA + Q + hX_{11} + N_1 + N_1^T]x(t) \\ &+x^T(t)[PBK + hA^TZBK - N_1 + N_2^T + hX_{12}]^Tx(t-\tau) + x^T(t-\tau)[PBK + hA^TZBK - N_1 + N_2^T + hX_{12}]^Tx(t) \\ &+x^T(t-\tau)[-N_2 - N_2^T - Q + hX_{22} + hK^TB^TZBKX_{12}]x(t-\tau) \\ &- \int_{t-\tau}^{t}[\dot{x}^TZ\dot{x}(s) + \xi^T(t)X\xi(t) + 2(x^T(t)N_1 + x^T(t-\tau)N_2)\dot{x}(s)]ds = \\ &\begin{bmatrix}x(t)\\x(t-\tau)\end{bmatrix}^T\begin{bmatrix}PA + A^TP + Q + hX_{11} & PBK - N_1 + N_2^T \\ +N_1 + N_1^T + hA^TZA & +hX_{12} + hA^TZBK \\ * & -N_2 + N_2^T - Q \\ & +hK^TB^TZBK\end{bmatrix} \times \begin{bmatrix}x(t)\\x(t-\tau)\end{bmatrix}^T \\ &- \int_{t-\tau}^{t}\begin{bmatrix}x(t)\\x(t-\tau)\\\dot{x}(s)\end{bmatrix}^T \times \begin{bmatrix}X_{11} & X_{12} & N_1\\ * & X_{22} & N_2\\ * & * & Z\end{bmatrix}\begin{bmatrix}x(t)\\x(t-\tau)\\\dot{x}(s)\end{bmatrix}ds\end{aligned} \tag{16}$$

We also define eqs. (17) and (18):

$$\Xi = \begin{bmatrix}PA + A^TP + Q + hX_{11} & PBK - N_1 + N_2^T \\ +N_1 + N_1^T + hA^TZA & +hX_{12} + hA^TZBK \\ * & -N_2 + N_2^T - Q \\ & +hK^TB^TZBK\end{bmatrix} \tag{17}$$

$$\Psi = \begin{bmatrix}X_{11} & X_{12} & N_1\\ * & X_{22} & N_2\\ * & * & Z\end{bmatrix} \tag{18}$$

It can be seen from eq. (16) that if it is $\Xi < 0, \Psi > 0$, then it is $\dot{V}(x_t) < 0$ and this means that the closed loop system of eq. (8) is stable. Next, based on Lemma 1, $\Xi < 0$ can be easily provided in relation (19):

$$\Xi = \begin{bmatrix}PA + A^TP + Q + hX_{11} + N_1 + N_1^T & PBK - N_1 + N_2^T + hX_{12} & hA^TZ \\ * & -N_1 + N_2^T - Q + hX_{22} & hK^TB^TZ \\ * & * & -hZ\end{bmatrix} < 0 \tag{19}$$

To obtain the K gain of the controller, it is necessary to use the following definitions:

$$\begin{aligned}&L = P^{-1}, M_1 = P^{-1}N_1P^{-1}, M_2 = P^{-1}N_2P^{-1}, R = Z^{-1}, V = KP^{-1}, Q_1 \\ &= P^{-1}QP^{-1}, Y = diag\{P^{-1}, P^{-1}\}Xdiag\{P^{-1}, P^{-1}\}\end{aligned}$$

By multiplying the right-hand and left-hand sides of eq. (19) by $diag\{P^{-1}, P^{-1}, Z^{-1}\}$, eq. (20) is extracted:

$$\begin{aligned}\Xi &= \begin{bmatrix}P^{-1} & 0 & 0\\ 0 & P^{-1} & 0\\ 0 & 0 & Z^{-1}\end{bmatrix}\begin{bmatrix}PA + A^TP + Q + hX_{11} + N_1 + N_1^T & PBK - N_1 + N_2^T + hX_{12} & hA^TZ \\ * & -N_1 + N_2^T - Q + hX_{22} & hK^TB^TZ \\ * & * & -hZ\end{bmatrix} \\ &\times \begin{bmatrix}P^{-1} & 0 & 0\\ 0 & P^{-1} & 0\\ 0 & 0 & Z^{-1}\end{bmatrix} = \begin{bmatrix}AL + LA^T + Q_1 + hY_{11} + M_1 + M_1^T & BV - M_1 + M_2^T + hY_{12} & hLA^T \\ * & -M_2 - M_2^T - Q_1 + hY_{22} & hV^TB^T \\ * & * & -hR\end{bmatrix} < 0\end{aligned} \tag{20}$$

Obviously, eq. (19) becomes equivalent to (9). Similarly, by multiplying the sides of eq. (18) by $diag\{P^{-1},P^{-1},P^{-1}\}$, eq. (18) becomes equivalent to (10). Therefore, the proof of theorem 1 is completely finished.

According to the definition of Theorem 1, eq. (10) can no longer be called an LMI due to the nonlinear conditions of $LR^{-1}L$, and therefore we cannot use a convex optimization algorithm to find a minimum value. For this reason, this paper uses cone complementarity linearization algorithm so that this algorithm is able to solve LMI [27]. Based on this, we can define the nonlinear optimization problem and its related constraints as (21):

$$
\begin{aligned}
&Minimize \quad tr\{FF_1+LL_1+RR_1\}\\
&Subject \quad to:\\
&\begin{bmatrix} AL+LA^T+Q_1+hY_{11}+M_1+M_1^T & BV-M_1+M_2^T+hY_{12} & hLA^T \\ * & -M_2-M_2^T-Q_1+hY_{22} & hV^TB^T \\ * & * & -hR \end{bmatrix} <0\\
&\begin{bmatrix} Y_{11} & Y_{12} & M_1 \\ * & Y_{22} & M_2 \\ * & * & F \end{bmatrix} >0\\
&\begin{cases} \begin{bmatrix} F & I \\ I & F_1 \end{bmatrix} >0, \begin{bmatrix} F_1 & L_1 \\ L_1 & R_1 \end{bmatrix} >0 \\ L>0, F>0, R>0 \end{cases}
\end{aligned}
\tag{21}
$$

In the following, according to the mentioned non-linear optimization process, the optimal gain matrix of the controller as well as the maximum value of the $h=\max(\tau)$ delay margin can be searched using the iterative algorithm proposed below.

Algorithm solution process:

Step 1: First, a small initial value for the delay margin should be chosen so that it can satisfy the feasibility region for relations (9) and (21).

Step 2: First, a set of possible matrix variable values should be set for $(L^{'},L_1^{'},V^{'},M_1^{'},M_2^{'},F^{'},F_1^{'},Q_1^{'},R^{'},R_1^{'},Y^{'})$, so that it satisfies eqs. (9) and (21), and then k = 0 is set.

Step 3: Solving the aforementioned nonlinear optimization problem with the constraints of LMIs in eqs. (9) and (21) and then setting:

$$F_{k+1}=F, F_{1,k+1}=F_1, L_{k+1}=l, l_{1,k+1}=L_1, R_{k+1}=R, R_{1,k+1}=R_1.$$

Step 4: If the inequality (10) is possible, increase the scalar value h to a small amount and then return to step 2. Stop if inequality (10) is not feasible in a certain number of iterations. And otherwise, set step $k=k+1$ and go to step 3.

Therefore, according to theorem 1 and the aforementioned algorithm, we will be able to obtain the optimal benefit of the feedback controller along with the maximum delay margin.

2.3. C. Observer-based state feedback design

In practical power systems, because the working state variables are not fully observed, it is usually preferred to use a feedback controller with measurable variables. For this purpose, O(s) state observation is introduced to observe transition state variables by WAMS. In this paper, the mode viewer is designed using the conventional pole placement method [23]. In Fig. 1, the structure of the state observer in the WADC design is shown. In this case, the design process is done in two stages:

Step 1: determining a state feedback gain matrix for the desired poles of the system.

Step 2: determination of an observer's gain matrix for optimal placement of the observer's poles.

By combining the state space equations of the system and the observer equations and by defining the $e(t)$ error signal (difference between the actual and estimated signal), we will have (22):

$$
\begin{bmatrix} \dot{x}(t) \\ \dot{e}(t) \end{bmatrix} = \begin{bmatrix} A-BK & BK \\ 0 & A-LC \end{bmatrix} \begin{bmatrix} x(t) \\ e(t) \end{bmatrix} \tag{22}
$$

Eq. (22) describes the dynamics of a closed loop system with a state feedback controller and an observer. Therefore, the characteristic equation of the closed loop system is (23):

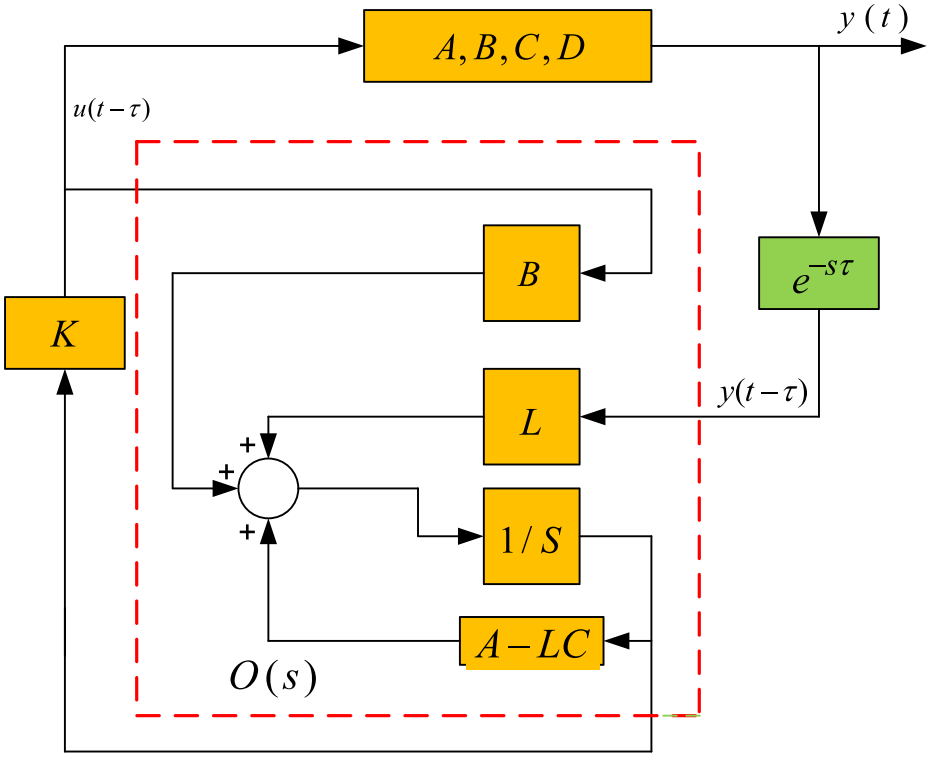

Fig. 1. Structure of state observer in WADC design for closed loop system.

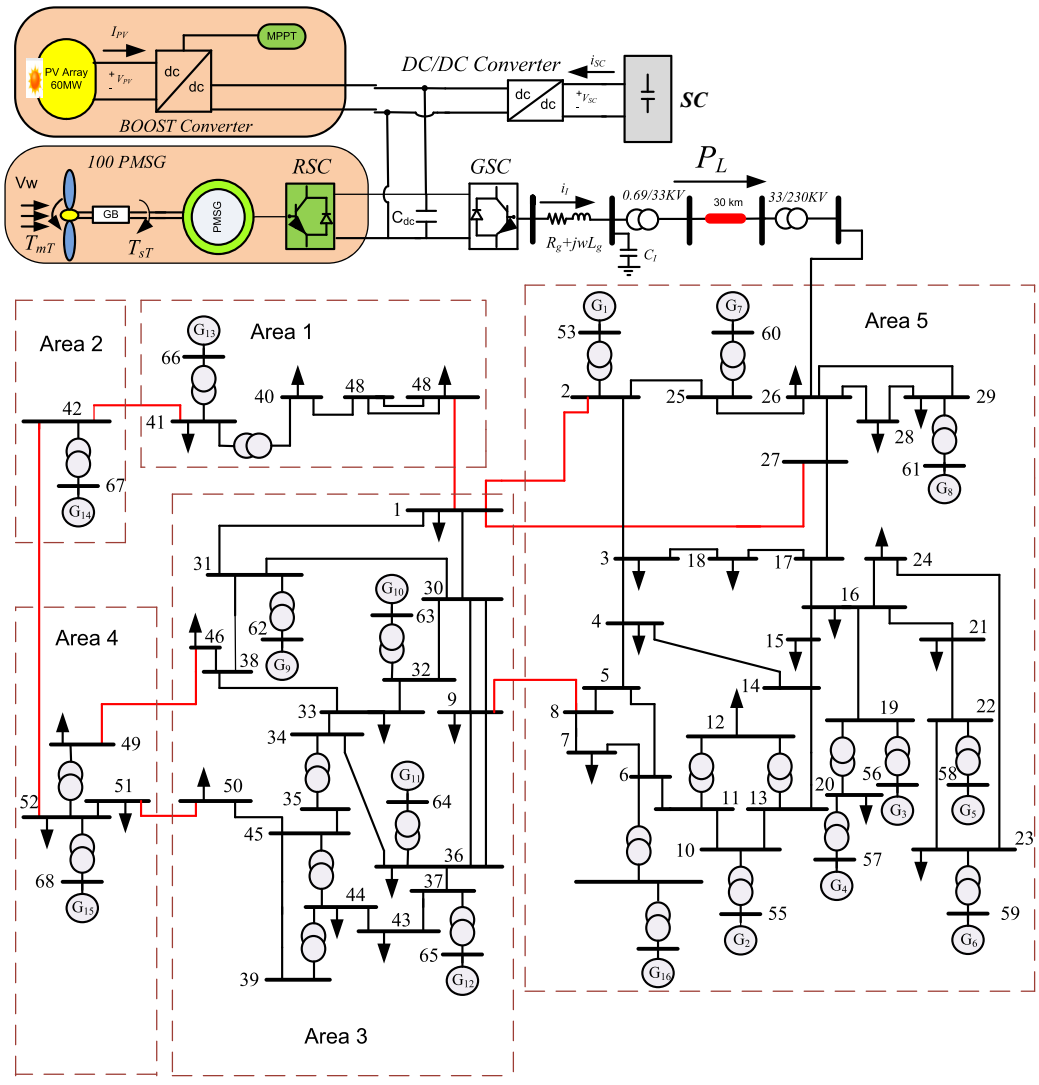

Fig. 2. Single-line diagram of the power system under study.

$$\begin{vmatrix} sI - A + BK & -BK \\ 0 & sI - A + LC \end{vmatrix} = 0 \tag{23}$$

And as a result we will have (24):

$$|sI - A + BK||SI - A + LC| = 0 \tag{24}$$

Therefore, the closed loop poles of the state feedback control system with the observer are formed from the sum of the poles resulting from the state feedback design and the observer design. This means that the design of the observer and the positioning of the pole with mode feedback are done separately and independently from each other.

The desired poles of the closed loop (caused by the state feedback) are determined in such a way that the performance characteristics of the closed loop system are met. The poles of the observer are also determined in such a way that the response of the observer is much faster than the response of the system. A rule of thumb for determining the location of observer poles is to choose them in such a way that the response of the observer is 2 to 10 times faster than the response of the system. Therefore, in this paper, by forming state and observability matrices in MATLAB software, it is possible to obtain the sum of closed loop poles with state and observer feedback. Therefore, first, the closed loop poles of the system are extracted using the command P = eig(A) in MATLAB software, and considering that we need the dynamics of the observer to be faster than the system itself, the poles of the observer must be at least 3 times farther from be the dominant poles of the system. Therefore, after obtaining the dominant poles of the system as P = eig(A) and placing these poles with a factor of 3 times farther from P as P_1, the gain of the observer can be extracted using the $L = place(A', C', P_1)$ command.

In this paper, for gain K, we will have feedback according to the proposed controller and for gain L, we will have an observer in MATLAB software:

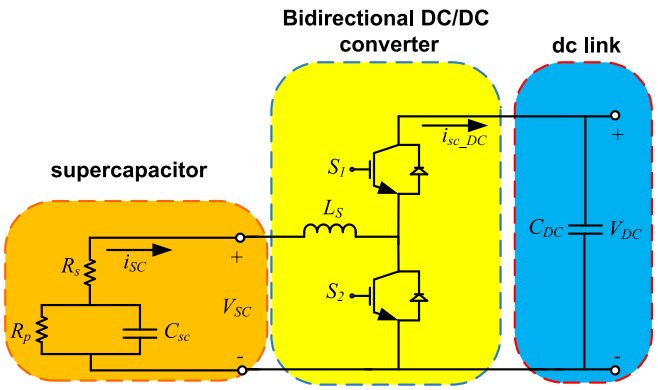

Fig. 3. Circuit structure of bidirectional dc/dc converter with energy storage.

$$K = \begin{bmatrix} -0.6578 & 1.3214 & -7.2346 & 5.1104 & 0.5467 & 2.3791 & 4.3639 & -3.6218 & 0.6435 & 0.1654 & -0.5672 & 3.4562 & -2.4567 \\ -0.7891 & 1.0678 & 5.3211 & -0.9875 & -1.8976 & 1.7654 & -5.6784 & -4.4566 & 1.3211 & 0.8745 & 0.5678 & -1.4567 & -1.0678 \end{bmatrix}^T$$

$$L = \begin{bmatrix} -2.4501 & -1.5647 & -2.7716 & -1.6557 & -3.8121 & -2.3116 & -0.7891 & -2.3456 & -0.9876 & -1.1245 & -2.1456 & -1.5431 & -0.5671 \\ -1.9123 & -1.5671 & -2.0677 & -1.9544 & -2.7891 & -1.766 & -1.7654 & -0.5456 & -2.5671 & -2.5673 & -1.7893 & -3.456 & -1.0543 \end{bmatrix}^T$$

3. The power system under study

According to Fig. 2, in this paper, the power system of 16- machines and 68 buses is used as a large-scale power system connected to a wind unit based on a PMSG, PV and BESS. Power system information is reported in [28]. According to Fig. 2, in this power system, PV and PMSG units are connected to bus 26 of the power system through a 30 km long transmission line. So that PMSG unit has a capacity of 100 MW and PV array has a capacity of 60 MW. In this connection, PMSG and PV array are connected to each other through a voltage source converter and boost converter, respectively. In addition, in order to reduce the fluctuations of wind and PV units, BESS equipped with super capacitor (SC) has been used bidirectional in the DC link. Based on the results of modal analysis on the system under study, there is an inter-area mode (with an oscillation frequency of 0.57 Hz and a damping ratio of 0.017) between generators 10 and 14 in certain operating conditions. For such low frequency oscillation, WADC based complementary controller strategy for energy storage converter is better than local PSSs. However, it should be noted that for effective application of WADC, appropriate wide feedback signals should be selected first. In this regard, based on the joint Controllability and observability index (JCOI) [29], the changes in the power of $P_{1\text{-}48}$ lines have a higher visibility than the active power of other lines, so it has been used as a selected candidate for the stabilizing feedback signal to the WADC input. It should be mentioned that all synchronous generators are modeled with 5th order dynamic model, wind unit with 4th order model, BESS unit with 3rd order and PV unit with 1st order model. By specifying the input vector $U = [\Delta V_R, \Delta P_S]$ and the output vector $Y = [\Delta E_{fd}, \Delta v_{dl}]$, it is possible to reduce of the system model to 13th order by using the Schur reduction model. For this purpose, the Schur complement in the Robust MATLAB Simulink toolbox was used [26]. It is worth mentioning that local PSS is installed on generators (G_1, G_4, G_8, G_9, G_{12}, G_{13}, G_{14}, G_{15}, G_{16}) by default. For the purpose of comparison, in addition to the WADC controller design, the classical power oscillation damping (CPOD) controller with P_L input (specified in Fig. 2) has been used as a local signal in BESS. Because this controller is fed through the local signal, it has no time delay and the structure of this controller is shown in the appendix section.

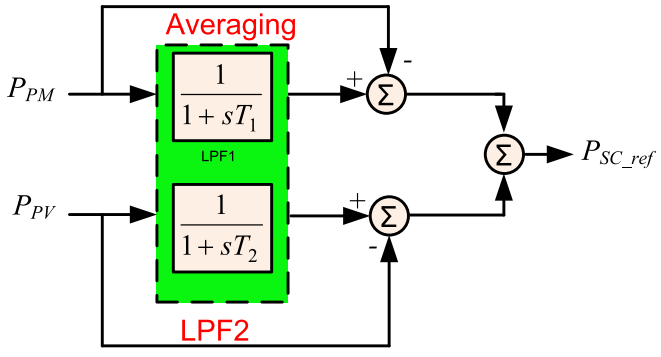

Fig. 4. Power control loop for PV and PMSG.

3.1. A. The model related to PMSG, PV and BESS converter units

In this paper, reference [30] models and mathematical relationships have been used for the PMSG unit and [31] for the PV unit.

Fig. 3 shows the circuit model for the bidirectional DC/DC converter equipped with SC. It can be seen that this converter has two switches S_1 and S_2 along with an energy storage inductor [31]. The structure of the used converter is such that it can be operated in both Buck and Boost modes.

According to the average value of the dynamic model, the output current of this converter is equal to [20]:

$$\frac{di_{sc}}{dt} = \frac{1}{L_S}(V_{SC} - f_S V_{DC} - R_S i_{SC}) \tag{25}$$

$$i_{SC\_DC} = f_S i_{SC} \tag{26}$$

In which, if it is $f_S = D_S$, the converter will work in Buck mode, and if it is $f_S = 1 - D_S$, the converter will work in Boost mode. According to the equivalent circuit in Fig. 3, the dc link voltage is equal to [20]:

$$\frac{dV_{C_{SC}}}{dt} = \frac{1}{C_{SC}}(-i_{SC} - \frac{V_{C_{SC}}}{R_{P_{SC}}}) \tag{27}$$

$$V_{SC} = V_{C_{SC}} - R_{S_{SC}} i_{SC} \tag{28}$$

Due to the fluctuating nature of wind in PMSG as well as variations in solar radiation in PV, the power transferred to the dc link fluctuates. In order to be able to transfer a smooth and non-oscillating power to the AC network, it is necessary to adjust and compensate the SC power. In this regard, the controller of Fig. 4 has been used to compensate the input power to the inner loop, i.e. P_{SC_ref}. According to Fig. 4, the powers transferred to the DC link pass through a low-pass filter after measurement for averaging. Then the filtered signals are compared with the reference signals and P_{SC_ref} power is generated from the sum of the compared signals.

4. Simulation results

The structure of the closed loop system for simulations is shown in Fig. 5. In this structure, the loops related to the controllers and how they are related to the power system is specified. All the control loops including the BESS converter control loop along with the damping control loop, the PV converter control loop and the PMSG control loops in the rotor side converter (RSC) and the grid side are connected to each other through the DC link. The simulation results have been evaluated in the form of four scenarios, so that in this evaluation, the wind pattern for all four scenarios is according to Fig. 6.

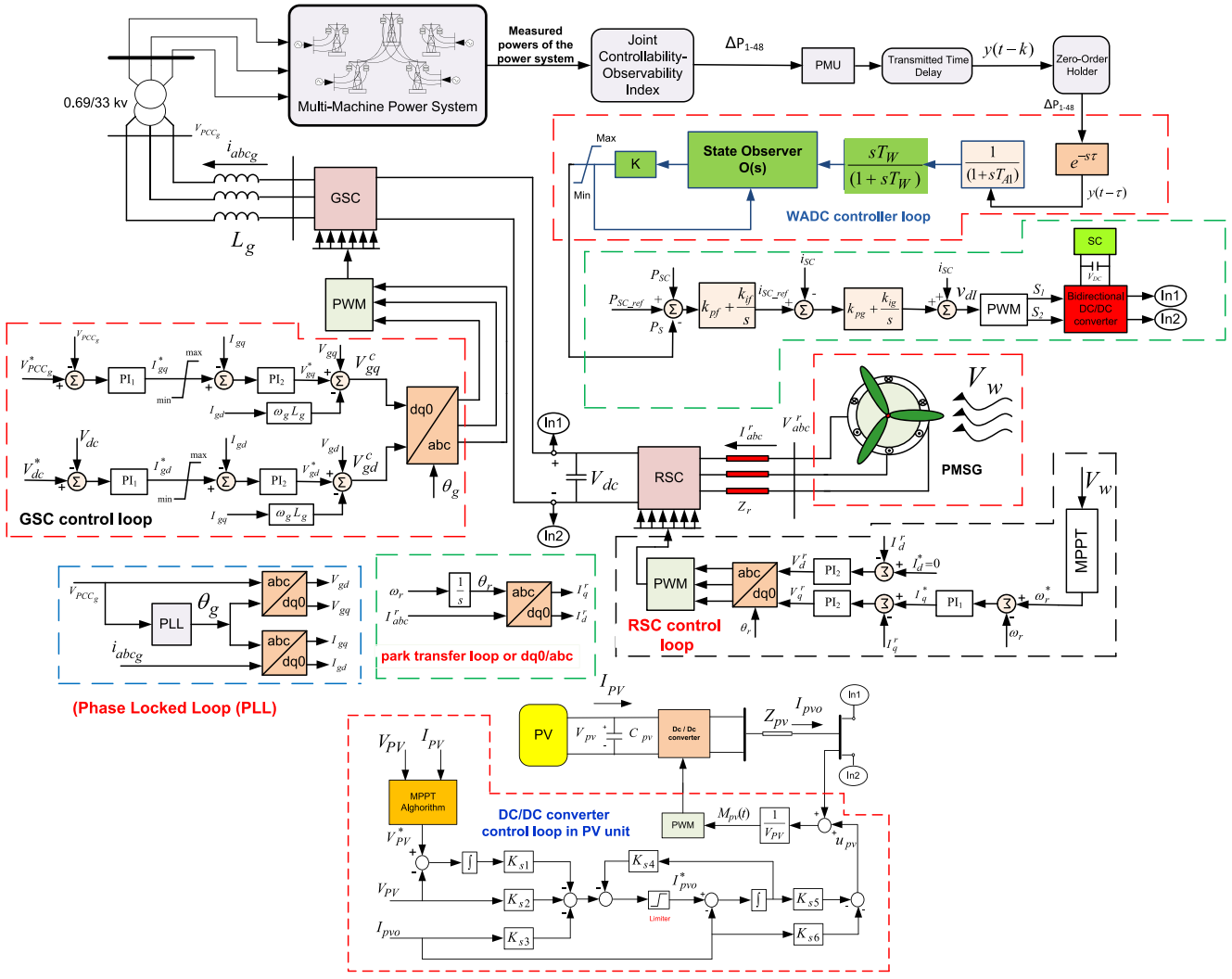

Fig. 5. The closed loop system of the proposed controller along with all the control loops of the converters.

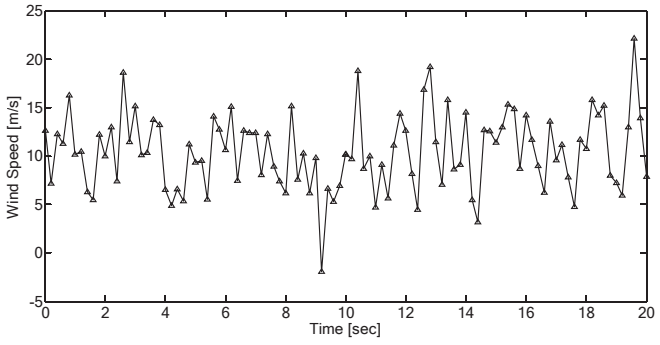

Fig. 6. Wind variation for PMSG unit.

4.1. Scenario 1

In this scenario, we apply a three-phase short-circuit fault temporarily for 0.1 s near bus 11 (between lines 11–12). The wind pattern is as shown in Fig. 6 and the solar radiation is considered constant and equal to 1000 degrees Celsius. Accordingly, in Fig. 7(a) and 7(b), respectively, the changes in the output power of the wind unit and the response of the active power of line 1–48 are shown by applying a time delay of 100 ms in sending remote signals to the WADC. It can be seen from the results of this response, even if there is a time delay, the WADC controller provides better stability than the CPOD method. Also, in Fig. 7(c) and 7(d), the DC link voltage and the power changes of the inter-area line 1–27 per time delay of 100 ms are shown, respectively. From the results of this scenario, it can be seen that the proposed controller for damping power fluctuations has a favorable performance against uncertainties caused by time delay and three-phase fault. This improvement is clearly seen both in the settling time and in overshoot and undershoots.

4.2. Scenario 2

In this scenario, a three-phase fault occurred permanently near bus 31 (between line 31 and 38) within 2 s, and because the fault was not resolved after 0.1 s, line 31–38 was outage. In addition, by changing the input mechanical power of the generators (G_1, G_4, G_8, G_{10}, G_{12}) by + 10 % and considering the wind and sun pattern as in the scenario 1, the simulation results have been evaluated. Based on this, the speed deviation of generators 6–14 in Fig. 8 (a), the power changes of line 14–15 in Fig. 8 (b), the PV output power in Fig. 8(c), as well as the power changes of line 8–9 in Fig. 8 (d) is shown for time delays of 300 ms. From these results of this scenario, it is clearly seen that the proposed controller is optimal under any conditions and provides the desired stability for the system. If in the case without a controller, the oscillations caused by uncertainties are not well damped and the stability of the system decreases with the passage of time.

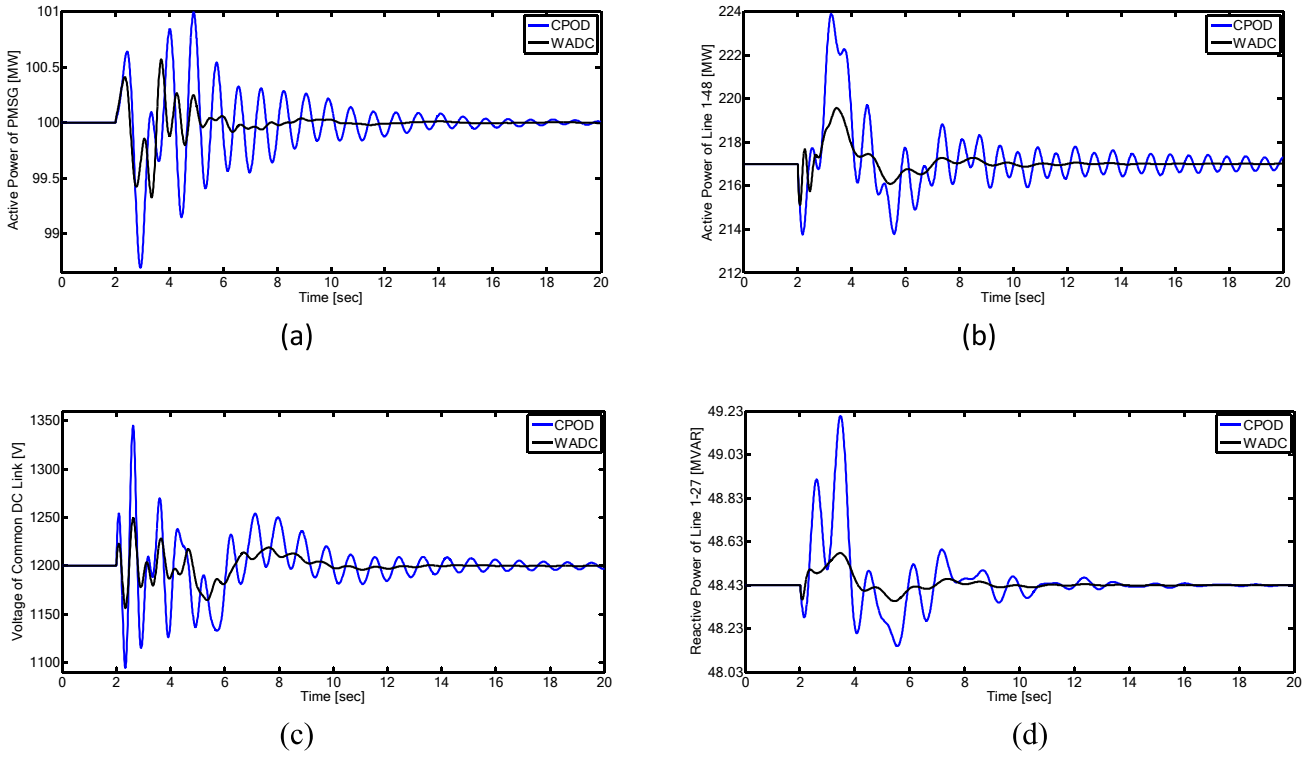

Fig 7. Simulation results for the scenario 1.

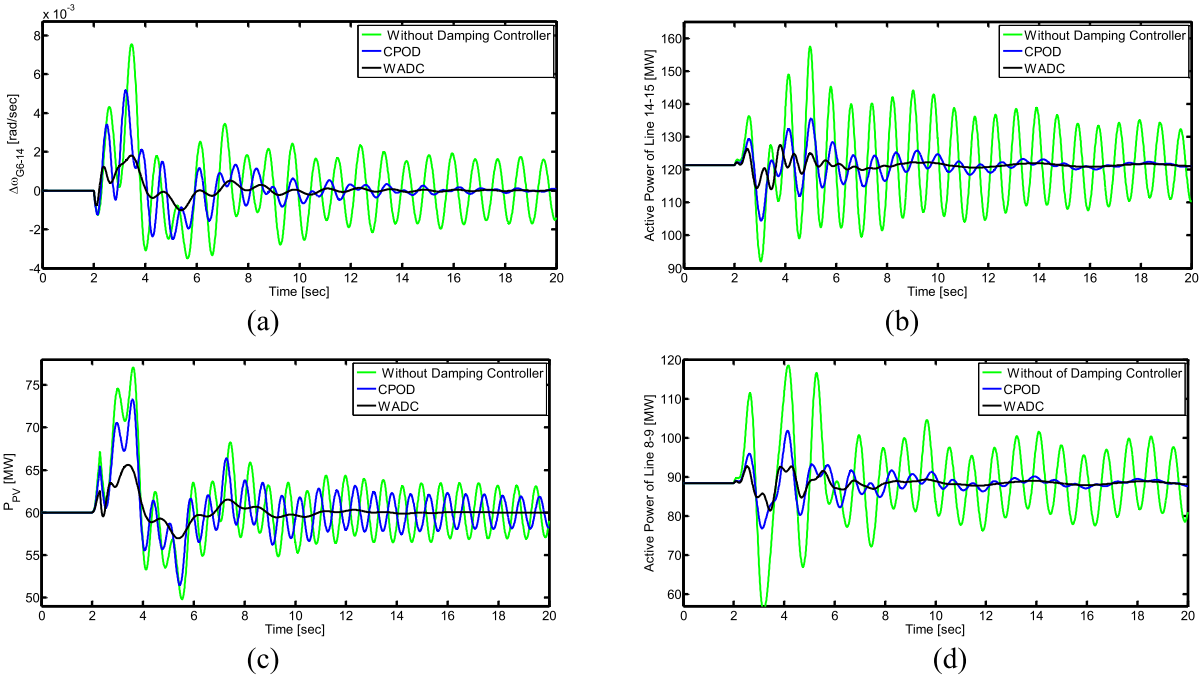

Fig. 8. Simulation results for the scenario 2.

4.3. Scenario 3

In this scenario, a three-phase fault has occurred permanently near bus 4 between lines 4–14 in 2 s. The duration of the fault is 0.1 s. But due to the fault not disappearing, the 14–4 line has been outage. Considering the wind pattern as in the scenario 1 and the changes in solar radiation as shown in Fig. 9(a), the simulation results have been evaluated considering time delays of 200 ms. Based on this, the power changes of line 9–5 are shown in Fig. 9(b), the speed deviation response of generators 7–15 in Fig. 9(c) and the power changes of PV unit are shown in Fig. 9(d). From the results of this scenario, it is clearly seen that even in the case of solar radiation changes, the proposed controller shows a very favorable performance in improving the damping of fluctuations.

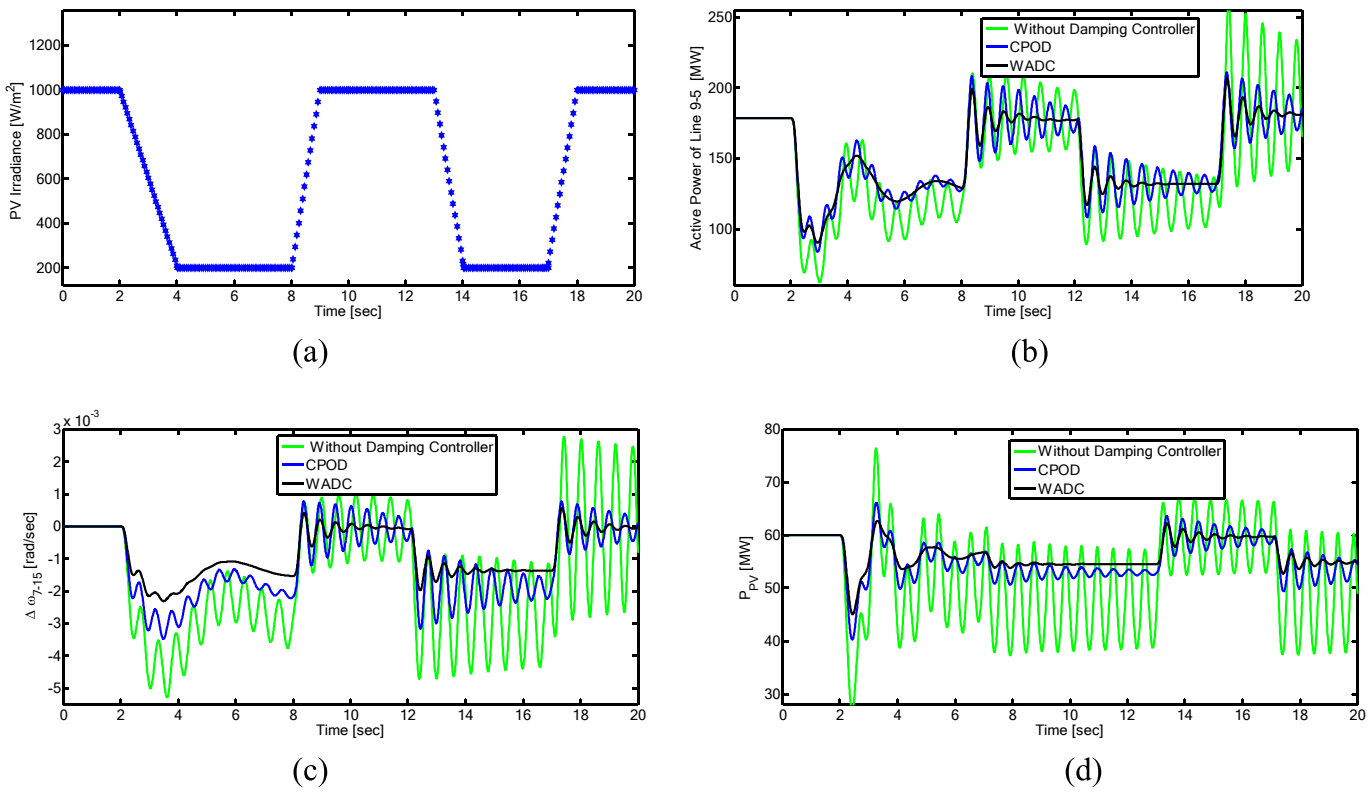

Fig. 9. Simulation results for the scenario 3.

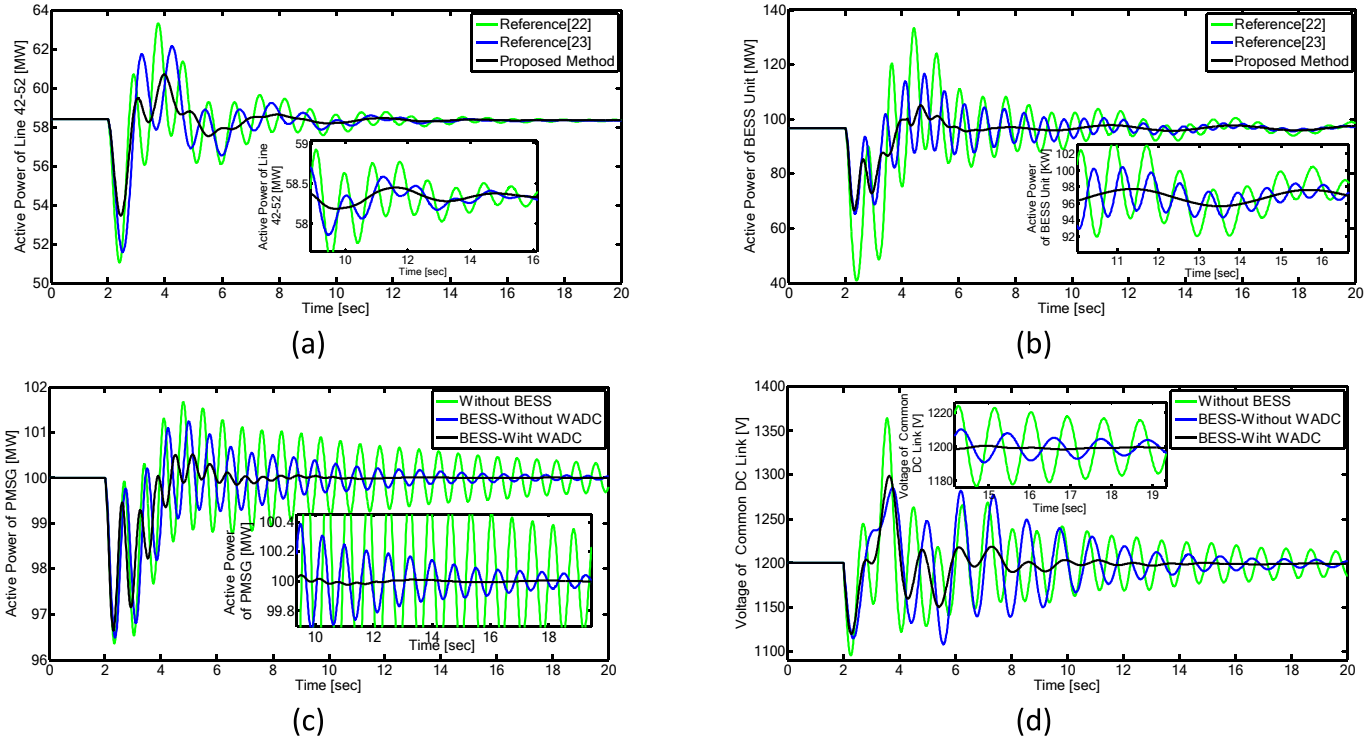

Fig. 10. Simulation results for the scenario 4.

4.4. Scenario 4

In this section, in order to show the better performance of the proposed controller compared to references [22,23], the simulation results have been analyzed. Therefore, by applying a permanent three-phase short-circuit fault in 2 s near bus 2 (between line 2 and 3), line 2–3 is outage after 0.1 s due to the fault not being resolved. The pattern of wind blowing and solar radiation is the same as the scenario 1 and the change

Table 1
Information about controllers and their related parameters.

Operating conditions at different work points	The active power of the energy storage unit in MW	The active power of the photovoltaic unit in MW	Reactive power of wind unit in MVAR	Active power of wind unit in MW	Solar radiation in degrees Celsius	The rotor speed of the wind unit in p.u	Wind speed in m/s
Subsynchronous mode	50	40	55	65	700	0.729	9
Super synchronous mode	97	55	61	100	1200	1.15	14
Synchronous mode	97	60	38.9	100	1000	1	12
Random mode	97	59.2	48.4	100	Fig. 9(a)	1.1	Fig. 6

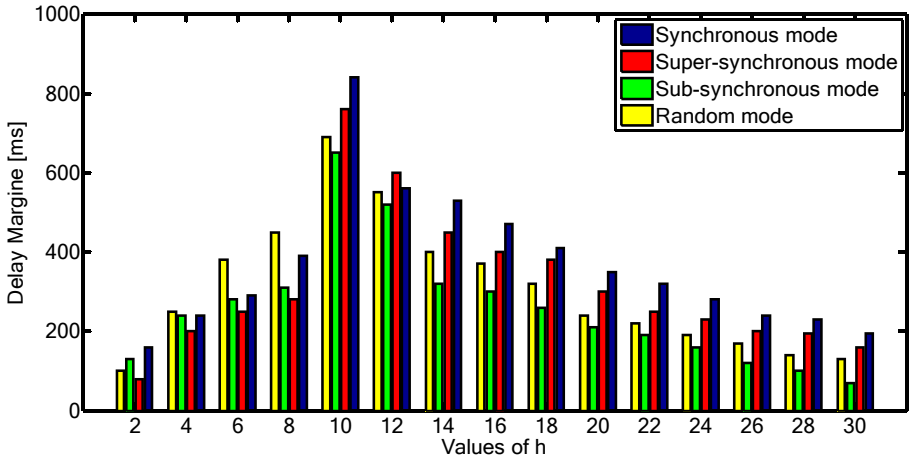

Fig. 11. Comparison of the changes related to the delay margin for different scalars.

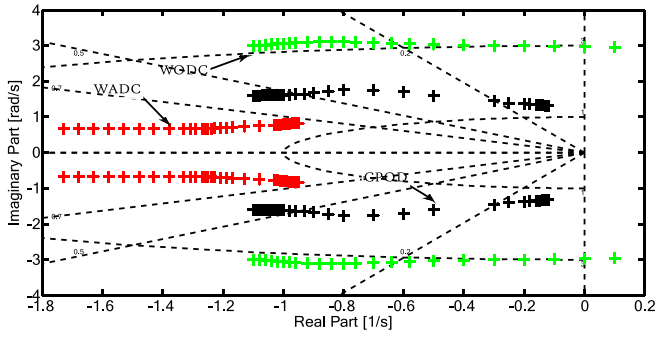

Fig. 12. Placement of oscillatory modes in the Complex plane under the scenario 1.

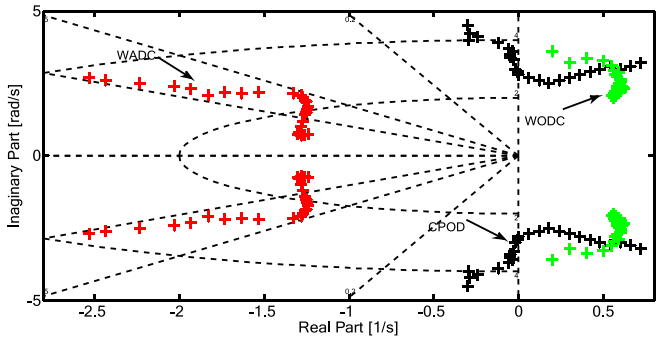

Fig. 13. Placement of oscillatory modes in the Complex plane under the scenario 2.

in the input mechanical power of the generators (G_1, G_5, G_{11}, G_{40}) is considered to be + 15 %. Based on this, Fig. 10(a) and 10(b) show the changes of active power between line 42–52 and BESS output power per time delay of 300 ms, respectively. From these figures, it can be seen that the improvement of oscillation damping in the proposed method is much more favorable and faster than the other two references, which has led to the reduction of settling time, overshooting and undershooting. Fig. 10(c) and 10(d) show the changes in the active power of the wind unit and the changes in the DC link voltage due to the entry and exit of the BESS, respectively. From these problems, it can be seen that as a result of the BESS unit leaving the network, the line power and link voltage are greatly affected, which leads to a decrease in the stability of the power system. This is despite the fact that in the presence of the BESS unit, even if there are time delays of 300 ms in the input of the WADC, a much more favorable damping is provided compared to the absence of the BESS. Therefore, the impact of the battery energy storage system in connecting to the DC link is very important, so that the power fluctuations of the renewable units can be improved through the BESS controller.

4.5. D. Examining the stability criteria of theorem 1 and choosing the appropriate scalar h

In order to provide a larger delay margin as well as the optimality of the proposed controller under different operating conditions (referred to in Table 1), the appropriate *h* should be selected by trial and error. For this purpose, in Fig. 11, for different values of the scalar h, the value of the margin of delay under different working points of the power system has been obtained. As can be seen from Fig. 11, if the *h* value is chosen equal to 10, a larger delay margin will be created for the controller, which provides sufficient assurance for the operation of the power system from the point of view of the time delay. Therefore, in the present work, the gain of the controller has been obtained by selecting *h* equal to 10.

4.6. E. Analysis of the sensitivity and stability of the controller to the changes in parameters and operating points of the system

In this section, in order to further investigate the stability of the proposed controller under changes in system operating points and the sensitivity of parameters due to uncertainties for power system oscillatory modes, an analysis has been carried out according to the following scenarios, the purpose of which is to The optimality of the proposed controller for the gain K(s) obtained should be confirmed. Therefore, based on the closed loop system of Fig. 5 and placing K(s) in the supplementary control loop of BESS, we will have:

4.7. Scenario 1

In this scenario, with a change in the mechanical power input of SG from −10 % to 10 % and a change in the impedance of the line connecting the renewable units to the power system by + 20 %, the root locus of the oscillating modes under normal operating conditions (synchronous mode) is shown in Fig. 12. In this figure, it can be seen that the oscillatory modes in the WADC mode are in the stable region with damping ratios above 5 %. While the oscillating modes in the design mode without damping controller (WODC) have ratios below 5 %, by applying more uncertainty, the location of the modes will be in the unstable region, which is shown in the second scenario of this position.

4.8. Scenario 2

The second scenario: in this scenario, with the pattern of wind speed as in Fig. 6, solar radiation as in Fig. 9(a), variable delay with time of 300 ms, and the outage of line 12–4, the root locus of the oscillating modes is shown in Fig. 13. It can be seen that even in the presence of various uncertainties; the WADC controller still has damping ratios above 5 %, which is in the stable region. Meanwhile, the CPOD controller has moved to the right side of the imaginary axis by applying more restrictions, which leads to a decrease in damping and, as a result, instability. Also, in the WODC mode, there is no stable region for power system oscillatory modes that have damping ratios higher than 5 %. It can be seen from both the above scenarios that the proposed controller will be stable under different working points of the power system.

5. Conclusion

In this paper, with the design of the WADC controller, the stability of the power system was evaluated using the FWM method under different scenarios. The FWM design method is solved by introducing a set of nonlinear matrix inequality constraints based on LMI constraints in the form of an optimization problem. In this method, by introducing the non-linear optimization algorithm, it can be used to search for the most optimal gain matrix and the maximum delay margin of the control signal. This design process is able to avoid the destructive effect of large amplitude time delays on the performance of the power system. Finally, the WADC controller design method was applied as a supplementary signal to the BESS converter to reduce the fluctuating performance of PV and wind units in the power system. The simulation results were tested on the improved power system of 16- machines using MATLAB software. From the results of this simulation, it is clearly seen that in the proposed method, in addition to improving the stability of the power system, the changes caused by time delays in sending signals from far away can be well controlled.

CRediT authorship contribution statement

Shuguang Li: Writing – original draft, Methodology, Investigation, Conceptualization. **Mohana Alanazi:** Writing – original draft, Software, Investigation, Funding acquisition. **Rasheed Abdulkader:** Writing – review & editing, Formal analysis, Data curation. **Mohamed Salem:** Writing – review & editing, Investigation, Formal analysis, Data curation. **Maher G.M. Abdolrasol:** Writing – review & editing, Methodology, Investigation. **Faisal A. Mohamed:** Writing – review & editing, Supervision, Methodology, Conceptualization. **Thamer A.H. Alghamdi:** Supervision, Resources, Funding acquisition, Conceptualization.

Declaration of competing interest

The authors declare that they have no known competing financial interests or personal relationships that could have appeared to influence the work reported in this paper.

Data availability

No data was used for the research described in the article.

Appendix 1. Adaptation of the proposed strategy for the system under study

In this section, to match the power system model with the proposed controller, network dynamic equations, including synchronous generators [28], wind power plant [30], PV unit [31], BESS [31] and damping controller are introduced. Therefore, for the closed loop system of relation (6) which is linearized under normal operating conditions (synchronous mode mentioned in Table 1), X is the system state vector, U is the input vector, and Y is the output state vector, which in this paper is They are defined as follows:

$$\begin{cases} X = \left[\Delta i_{dsw}, \Delta i_{qsw}, \Delta i_{drw}, \Delta i_{qrw}, \Delta E_D^{'}, \Delta E_Q^{'}, \Delta E_{fd}, \Delta\delta, \Delta\omega, \Delta i_{SC}, \Delta V_{CSC}, \Delta v_{dI}, \Delta V_{PV}\right]^T \\ U = [\Delta V_R, \Delta P_S] \\ Y = [\Delta E_{fd}, \Delta v_{dI}] \end{cases}$$

For the above vectors we will have:

$\Delta i_{dsw}, \Delta i_{qsw}, \Delta i_{drw}, \Delta i_{qrw}$: Corresponding to the stator and rotor currents of the wind unit in d and q axes, respectively.

$\Delta E_D^{'}, \Delta E_Q^{'}$: Corresponding to the electromotive force voltage of synchronous generators in d and q axes, respectively.

$\Delta E_{fd}, \Delta\delta, \Delta\omega, \Delta V_R$: Respectively related to excitation field voltage, rotor angle, rotor speed and supplementary signal of PSS controller in synchronous generators [32].

$\Delta i_{SC}, \Delta V_{CSC}, \Delta v_{dI}$: Respectively related to the current, voltage and switching signal of the PWM converter in the BESS control loop.

ΔV_{PV}: PV unit voltage.

ΔP_S: Supplementary damping controller signal sent through WADC to BESS.
The values of matrices A, B and C are equal to:

$$A = \begin{bmatrix}
1.2435 & 0.5671 & 0.1256 & 0.9801 & 0.3451 & 1.7654 & 0.4056 & 0.5674 & 0.7658 & 0.2345 & 0.6547 & 1.2087 & 0.5187 \\
0.4062 & 0.6134 & 1.8964 & 0.9380 & 0.5438 & 0.3275 & 0.5610 & 0.7403 & 1.5021 & 0.6581 & 0.8055 & 0.4328 & 0.6004 \\
0.7630 & 0.6543 & 0.6754 & 1.4571 & 1.5430 & 0.5611 & 0.1134 & 1.3267 & 1.2278 & 0.1087 & 1.5670 & 0.4328 & 0.5611 \\
1.3335 & 1.6533 & 0.7641 & 0.8904 & 1.8601 & 1.7773 & 0.8765 & 0.7653 & 0.4455 & 0.7655 & 0.6531 & 0.7004 & 0.7432 \\
0.4033 & 0.5427 & 1.6187 & 1.5890 & 0.9403 & 0.8126 & 1.2864 & 0.4243 & 0.5679 & 0.5428 & 0.6541 & 0.6507 & 1.4506 \\
0.6643 & 0.6782 & 0.8439 & 0.7901 & 1.8404 & 0.8175 & 0.5602 & 1.7632 & 0.8922 & 0.9027 & 0.8900 & 0.9764 & 0.9654 \\
0.8765 & 0.5431 & 1.7654 & 1.8612 & 0.4428 & 0.5670 & 1.4321 & 1.6643 & 0.8754 & 1.6540 & 0.6543 & 1.4328 & 0.7654 \\
0.5432 & 0.6704 & 0.4328 & 0.8953 & 1.7654 & 0.2109 & 0.5130 & 0.1986 & 0.2687 & 0.4356 & 1.7521 & 0.6705 & 1.7608 \\
0.5631 & 0.1778 & 0.5899 & 0.4332 & 0.6477 & 0.6728 & 0.8769 & 0.6654 & 1.1345 & 0.2876 & 0.5431 & 0.7567 & 0.8876 \\
0.4332 & 0.6088 & 1.4328 & 0.8601 & 0.7754 & 0.8658 & 1.4458 & 1.7765 & 0.3322 & 0.5548 & 0.8876 & 1.6654 & 1.8904 \\
0.6367 & 1.8654 & 0.6784 & 1.0876 & 0.5567 & 0.7439 & 0.8992 & 0.9701 & 1.0677 & 0.9978 & 0.3379 & 0.5543 & 0.8327 \\
1.0408 & 0.6648 & 0.3972 & 0.6520 & 1.1390 & 0.7694 & 0.4861 & 0.3863 & 0.8129 & 0.9411 & 0.6034 & 1.4561 & 0.8750 \\
0.6276 & 0.5399 & 0.6499 & 0.6781 & 0.7892 & 0.8904 & 0.7432 & 0.7894 & 0.6432 & 0.8902 & 1.432 & 1.167 & 0.6571
\end{bmatrix}$$

$$B = \begin{bmatrix}
0 & 0 & 0 & 0 & 0 & 0 & 0.9765 & 0 & 0 & 0 & 0 & 0 & 0 \\
0 & 0 & 0 & 0 & 0 & 0 & 0 & 0 & 0 & 0 & 0.8765 & 0 &
\end{bmatrix}$$

$$C = \begin{bmatrix}
0 & 0 & 0 & 0 & 0 & 0 & 0.6543 & 0 & 0 & 0 & 0 & 0 & 0 \\
0 & 0 & 0 & 0 & 0 & 0 & 0 & 0 & 0 & 0 & 0.9501 & 0 &
\end{bmatrix}$$

The structure of the CPOD controller is according to Fig. A1(a) of the appendix and it is used for the IEEE-1 type synchronous generator excitation system [32].

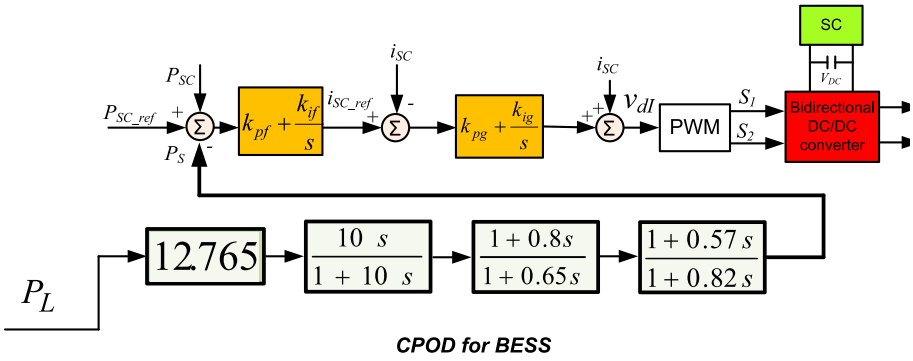

Fig. A1. (a) : Structure of CPOD controller for BESS

Appendix 2. The information related to the controller parameters is reported in Table 2

Table 2
Information about controllers and parameters related to them

Information about the BESS along with the controllers related to it			
R_s=0.1 Ω	R_p=0.04 Ω	L_s=4.5 mH	C_{sc}=75μf
T_W=10	T_{A1}=2.45	K_{pf}=6.65	K_{if}=3.15
K_{pg}=6.65	K_{ig}=6.65	(switching frequency) f=5 KH	
Power loop information for PV and PMSG			
T_1=3.87	T_2=2.55		
PV controller information			
Ks_1=7.4	Ks_2=2.5	Ks_3=3.8	Ks_4=5.5
Ks_5=1.6	Ks_6=3.9	(switching frequency) f=5 KH	V_{PV}=1200 (V)
Information about PMSG controllers			
PI_1:K_{p1}=4.65,K_{i1}=1.51	PI_2:K_{p2}=6.43,K_{i2}=2.32	$R_g+j\omega L_g$=0.86+j0.054ωΩ	$R_g+j\omega L_g$=0.22+j.0.18ωΩ

References

[1] Darabian M, Bagheri A. Stability improvement of large-scale power systems including offshore wind farms and MTDC grid aiming at compensation of time delay in sending robust damping signals. Int J Electr Power Energy Syst 2022 Dec;1(143):108491.

[2] Rafique Z, Khalid HM, Muyeen SM, Kamwa I. Bibliographic review on power system oscillations damping: an era of conventional grids and renewable energy integration. Int J Electr Power Energy Syst 2022;136:107556.

[3] Arrieta-Paternina, M. R., Franco, C., Zamora-Mendez, A., Mejia-Ruiz, G. E., Zelaya, F., Correa, R. E., ... & Segundo Sevilla, F. R. (2022). Enhancing Wide-Area Damping Controllers Via Data-Assisted Power System Linear Models. *Available at SSRN 4059938*.

[4] Ghaderi MH, Adelpour M, Rashidirad N, Hamzeh M. Analysis and damping of high-frequency oscillations at the presence of distributed constant power loads. Int J Electr Power Energy Syst 2020 Dec;1(123):106220.

[5] Ma J, Jie H, Zhou Y, Shao H, Zhao S, Du Y, et al. A low frequency oscillation suppression method for grid-connected DFIG with virtual inertia. Int J Electr Power Energy Syst 2023 Jan;1(144):108531.

[6] Krishnan VVG, Srivastava SC, Chakrabarti S. A robust decentralized wide area damping controller for wind generators and FACTS controllers considering load model uncertainties. IEEE Trans Smart Grid 2016;9(1):360–72.

[7] Darabian M, Bagheri A. Design of adaptive wide-area damping controller based on delay scheduling for improving small-signal oscillations. Int J Electr Power Energy Syst 2021 Dec;1(133):107224.
[8] Dörfler F, Jovanović MR, Chertkov M, Bullo F. Sparsity-promoting optimal wide-area control of power networks. IEEE Trans Power Syst 2014;29(5):2281–91.
[9] Zhou L, Yu X, Li B, Zheng C, Liu J, Liu Q, et al. Damping inter-area oscillations with large-scale PV plant by modified multiple-model adaptive control strategy. IEEE Trans Sustainable Energy 2017;8(4):1629–36.
[10] Li T, Hu W, Zhang B, Zhang G, Li J, Chen Z, et al. Mechanism analysis and real-time control of energy storage based grid power oscillation damping: a soft actor-critic approach. IEEE Trans Sustainable Energy 2021;12(4):1915–26.
[11] Björk J, Obradović D, Harnefors L, Johansson KH. Influence of sensor feedback limitations on power oscillation damping and transient stability. IEEE Trans Power Syst 2021;37(2):901–12.
[12] Xu X, Sun K. Direct damping feedback control using power electronics-interfaced resources. IEEE Trans Power Syst 2021;37(2):1113–25.
[13] Silva-Saravia H, Pulgar-Painemal H, Tolbert LM, Schoenwald DA, Ju W. Enabling utility-scale solar PV plants for electromechanical oscillation damping. IEEE Trans Sustainable Energy 2020;12(1):138–47.
[14] Bento ME. A hybrid particle swarm optimization algorithm for the wide-area damping control design. IEEE Trans Ind Inf 2021;18(1):592–9.
[15] Mukherjee S, Chakrabortty A, Bai H, Darvishi A, Fardanesh B. Scalable designs for reinforcement learning-based wide-area damping control. IEEE Trans Smart Grid 2021;12(3):2389–401.
[16] Isbeih YJ, Ghosh S, El Moursi MS, El-Saadany EF. Online DMDc based model identification approach for transient stability enhancement using wide area measurements. IEEE Trans Power Syst 2021 Jul 2;36(5):4884–7.
[17] Yao W, Nan J, Zhao Y, Fang J, Ai X, Zuo W, et al. Resilient wide-area damping control for inter-area oscillations to tolerate deception attacks. IEEE Trans Smart Grid 2021;12(5):4238–49.
[18] Wu W, Wang X, Rao H, Zhou B. Delay-dependent wide-area damping controller synthesis approach using jensen's inequality and evolution algorithm. CSEE J Power Energy Syst 2022.
[19] Sadiq R, Wang Z, Chung CY. A multi-model multi-objective robust damping control of GCSC for hybrid power system with offshore/onshore wind farm. Int J Electr Power Energy Syst 2023;147:108879.
[20] Prakash A, Kumar K, Parida SK. Energy capacitor system based wide-area damping controller for multiple inter-area modes. IEEE Trans Ind Appl 2022;58(2):1543–53.
[21] Pham TN, Oo AM, Trinh H. Event-triggered mechanism for multiple frequency services of electric vehicles in smart grids. IEEE Trans Power Syst 2021 Aug 2;37 (2):967–81.
[22] Sun Z, Zhao J, Long H. Design of a delay dependent wide area damping controller using cyber-physical power system architecture. Energy Rep 2023;9:510–7.
[23] Majumder R, Pal BC, Dufour C, Korba P. Design and real-time implementation of robust FACTS controller for damping inter-area oscillation. IEEE Trans Power Syst 2006;21(2):809–16.
[24] Liu Y, Hu Z, Suo J, Dong J. Design method of wide-area damping controller based on FOA algorithm. InProceeding of the 11th World Congress on Intelligent Control and Automation 2014 Jun 29 (pp. 4893-4897). IEEE.
[25] Fridman E, Shaked U. Delay-dependent stability and H∞ control: constant and time-varying delays. Int J Control 2003;76(1):48–60.
[26] Gao H, Lam J, Wang C, Wang Y. Delay-dependent output-feedback stabilisation of discrete-time systems with time-varying state delay. IEE Proceedings-Control Theory and Applications 2004;151(6):691–8.
[27] Sadabadi MS, Peaucelle D. From static output feedback to structured robust static output feedback: a survey. Annu Rev Control 2016;42:11–26.
[28] Shayeghi H, Ghasemi A. A multi objective vector evaluated improved honey bee mating optimization for optimal and robust design of power system stabilizers. Int. J. Electr. Power Energy Syst. 2014;62:630–45.
[29] Surinkaew T, Ngamroo I. Adaptive signal selection of wide-area damping controllers under various operating conditions. IEEE Trans. Ind. Inf. 2017;14(2): 639–51.
[30] Zhou D, Blaabjerg F, Franke T, Tønnes M, Lau M. Comparison of wind power converter reliability with low-speed and medium-speed permanent-magnet synchronous generators. IEEE Trans. Ind. Electron. 2015;62(10):6575–84.
[31] Samosir AS, Yatim AHM. Implementation of dynamic evolution control of bidirectional DC–DC converter for interfacing ultracapacitor energy storage to fuel-cell system. IEEE Trans. Ind. Electron. 2010;57(10):3468–73.
[32] Vittal V, McCalley JD, Anderson PM, Fouad AA. Power system control and stability. John Wiley & Sons; 2019 Oct 15.